Economic Geology, v. 113, no. 3, pp. 769–778

SCIENTIFIC COMMUNICATIONS

ANDRADITE GARNET U-Pb GEOCHRONOLOGY OF THE BIG GOSSAN SKARN, ERTSBERG-GRASBERG MINING DISTRICT, INDONESIA

S. Wafforn,[1,†] S. Seman,[2] J. R. Kyle,[1] D. Stockli,[1] C. Leys,[3] D. Sonbait,[3] and M. Cloos[1]

[1] *Department of Geological Sciences, Jackson School of Geoscience, University of Texas at Austin, Austin, Texas 78712–1692*

[2] *407 Deike Bldg., University Park, Pennsylvania State University, Pennsylvania 16802*

[3] *Freeport-Indonesia, Tembagapura, Papua 99920, Indonesia*

Abstract

The Big Gossan skarn (71 million tonnes of 2.4 wt % Cu and 0.9 ppm Au at a 1% Cu cutoff) is located in the prolific Ertsberg-Grasberg mining district, on the island of New Guinea in eastern Indonesia. The skarn formed within the steeply dipping southern limb of the Yellow Valley syncline near the conformable contact between the Cretaceous Ekmai limestone and Paleocene Waripi dolomitic limestone, adjacent to the western edge of the 3.1 to 2.8 Ma Ertsberg diorite. Andradite garnets from eight Big Gossan samples were directly dated using the laser ablation-inductively coupled plasma-mass spectrometry U-Pb method, and the age results show that Big Gossan formed between 2.9 and 2.7 Ma. To evaluate reproducibility, one sample was dated twice, four months apart, and gave overlapping ages of 2.75 ± 0.03 (n = 150 spots) and 2.73 ± 0.06 Ma (n = 50 spots) (lower intercept age, Tera-Wasserburg concordia). This precision was achievable due to the high U content (10–100 ppm) and single isotopic composition of common Pb in the Big Gossan garnets. Andradite garnet U-Pb ages are compatible with district-wide zircon U-Pb geochronology and a single 2.82 ± 0.04 Ma phlogopite $^{40}Ar/^{39}Ar$ age for the skarn. The new garnet ages confirm that Big Gossan was one of the last ore-forming events in the Ertsberg-Grasberg district. This study demonstrates that andradite garnet U-Pb chronometry can be a robust dating technique for constraining the timing of skarn-forming hydrothermal systems.

Introduction

Skarn ore deposits are major sources for a variety of metals, including Fe, Cu, Au, W, Mo, and rare earth elements (REEs). Cu- and Au-rich skarns commonly occur in the same mining districts as epithermal and porphyry Cu deposits (Sillitoe, 1993; Meinert et al., 2005), all of which are believed to form as a result of magmatic-hydrothermal fluid exsolution from an intermediate magma emplaced into the upper crust (Burnham, 1979; Candela, 1989; Hedenquist and Lowenstern, 1994). To form Cu-rich hydrothermal fluids, exsolution must occur at sufficient depths for chlorine, and thus Cu, to be partitioned into the fluid (Candela and Holland, 1984; Shinohara et al., 1989; Cline and Bodnar, 1991). Once Cu-rich hydrothermal fluids form at depth, bubble-bearing magma is able to rise until the expanding bubbles can separate and collect at the top of a stock (Cloos, 2001). Once a fluid-charged cupola is formed and a steady discharge is maintainable (e.g., Cloos and Sapiie, 2013), the main governing factor for whether porphyry- or skarn-type mineralization occurs is whether the metal-rich magmatic fluids pass through igneous or carbonate rocks (Meinert et al., 2003; Sillitoe, 2010). Skarn ore systems can be large (e.g., Ertsberg East; Leys et al., 2012) but can also have highly variable ore grades and complex mineralogy, making mining and beneficiation more difficult. Despite their potential challenges, skarn deposits represent attractive exploration targets for base and precious metals.

A major question in many skarn deposits is the timing of ore formation. Geochronology and thermochronology results from porphyry-related magmatic-hydrothermal systems, including zircon U-Pb, biotite Ar-Ar, and hornblende Ar-Ar ages, show that magmatic and hydrothermal activity may be episodic over millions of years (e.g., Chuquicamata, Ballard et al., 2001; El Teniente, Maksaev et al., 2004; Rio Blanco, Deckart et al., 2005) or may occur over a brief time period of 100,000 years or less (e.g., Potrerillos district, Marsh et al., 1997; Bajo de la Alumbrera, von Quadt et al., 2011; Far Southeast, Arribas et al., 1995). Similar detailed geochronology studies of skarn systems are rare, due to the scarcity of dateable primary skarn minerals, uncertainty regarding the related intrusions, or a lack of crosscutting relationships that directly constrain the duration of magmatic hydrothermal activity. Previous geochronological studies have largely focused on directly dating skarn mineralization, including Re-Os dating of molybdenite (e.g., Wan et al., 2014; Zhu et al., 2015), titanite (e.g., Chiaradia et al., 2009), and pyrrhotite (e.g., Wang et al., 2008), or dating lower temperature retrograde minerals such as phlogopite and muscovite by Ar-Ar methods (e.g., Peng et al., 2006; Xie et al., 2012). Two recent studies focused on dating hydrothermal zircon and baddeleyite using the laser ablation-inductively coupled plasma-mass spectrometry (LA-ICP-MS) U-Pb and secondary ion mass spectrometry (SIMS) U-Pb techniques (Deng et al., 2015; Zhao et al., 2016); however, hydrothermal zircon is uncommon. The abundance of garnets in skarn systems makes them potentially a much more effective mineral to determine the age and duration of skarn formation.

This study presents eight andradite garnet U-Pb ages from the Big Gossan skarn, located in the prolific Ertsberg-Grasberg mining district, on the Indonesian side of the island of

† Corresponding author: e-mail, swafforn@utexas.edu

ISSN 0361-0128; doi: 10.5382/econgeo.2018.4569; 10 p.
Supplementary files available online.

Submitted: June 19, 2017
Accepted: January 17, 2018

New Guinea (Leys et al., 2012). The young age of mineralization in the district (~3 Ma; McDowell et al., 1996; Wafforn, 2017) and lack of intense tectonic-magmatic-hydrothermal retrograde overprinting that affects many older skarn systems make it an excellent case study to test the potential of directly dating garnet. Ages were determined using LA-ICP-MS techniques, following the procedure described by Seman et al. (2017). Andradite garnets from Big Gossan proved to be well suited to dating using the LA-ICP-MS methodology, due to their relatively high U concentrations (10–100 ppm), relatively homogeneous distribution of U throughout the garnets, and consistent isotopic composition of the common Pb.

Geology of the Big Gossan skarn

The Big Gossan skarn is small compared to the giant Grasberg porphyry Cu deposit or the Ertsberg East skarn system (Fig. 1) but large compared to many Cu-bearing skarns (e.g., Meinert et al., 2005). It contains the highest average Cu grades in the mining district, with 71 million tonnes (Mt) at 2.4 wt % Cu and 0.9 ppm Au, at a cutoff grade of 1 wt % Cu (Leys et al., 2012). The Big Gossan skarn developed in the steeply dipping southern limb of the Yellow Valley syncline, near the contact between the Cretaceous Ekmai Formation and the Paleocene Waripi dolomitic limestone, close to the southwestern margin of the Ertsberg intrusion (Meinert et al., 1997). Structural analysis of the surrounding mine exploration and development drifts indicate the orebody (up to 1,100 m along strike, 4–60 m thick, and >700 m in vertical extent) is localized at the intersection between strike-slip faults (Gregory, 2004). In contrast to the other skarns in the Ertsberg-Grasberg district, including Dom, Ertsberg, Ertsberg East, and Kucing Liar (Mertig et al., 1994), Big Gossan is a garnet-pyroxene skarn, with a garnet to pyroxene ratio of 1:2. The predominant sulfide mineral is chalcopyrite, with local concentrations of up to 20% pyrite and <1% sphalerite, galena, and pyrrhotite.

For almost 25 years a single K-Ar age of 3.10 ± 0.12 Ma from an uncharacterized sample of the Ertsberg pluton, collected near the tramway terminal, was the primary constraint on the age of magmatism and mineralization in the Ertsberg-Grasberg mining district (Titley, 1975). McDowell et al. (1996) performed K-Ar dating of magmatic biotite from nine distinct intrusions in the district and found that magmatism occurred from 3.8 to 2.6 Ma. Biotite K-Ar results from the Ertsberg

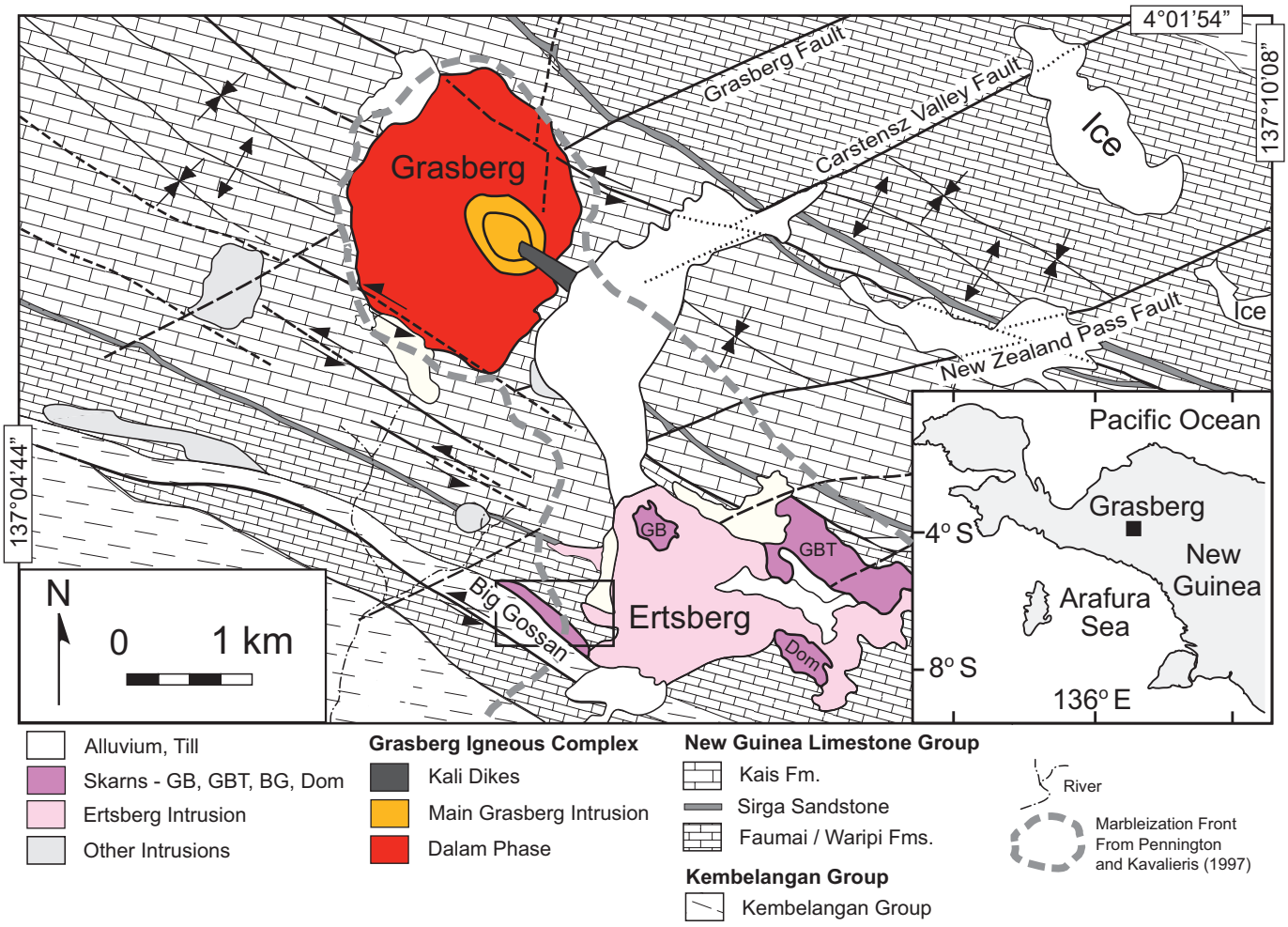

Fig. 1. Map of the Ertsberg mining district showing the location of the Big Gossan skarn. Modified from Paterson and Cloos (2005). Skarns: BG = Big Gossan, GB = Gunung Bijih, GBT = Gunung Bijih Timur (upper part of the Ertsberg East skarn system). Black box shows the location of the map in Figure 2.

pluton gave ages between 2.65 ± 0.12 and 3.09 ± 0.25 Ma. More recently, work was done to date every intrusion in the district using zircon U-Pb chronometry. The results confirm that magmatism in the district took place from 3.7 to 2.6 Ma (Wafforn, 2017). The only reported dating of the Big Gossan skarn is a single phlogopite $^{40}Ar/^{39}Ar$ age of 2.82 ± 0.04 Ma (Prendergast et al., 2005).

Previous work

Garnets are an attractive mineral phase to target for dating as they are ubiquitous in calc-silicate skarns, and the garnet-bearing mineral assemblage may record the P-T conditions of prograde metamorphic reactions (Burton and O'Nions, 1991; Baxter and Sherer, 2013). Dating garnets became possible in the 1990s due to improvements in mass spectrometry, with the most commonly used radiometric systems being Sm-Nd and Lu-Hf (Scherer et al., 2000; Smit et al., 2013). Mezger et al. (1989) made the first attempt to date garnets using the U-Pb radiometric system and the isotope dilution-thermal ionization mass spectrometry (ID-TIMS) method in order to assess the timing of staurolite breakdown during prograde metamorphism, the timing of migmatization, and the timing of late granitic intrusions in the Late Archean Pikwitonei granulite domain in Manitoba, Canada. Meinert et al. (2001) were the first to report garnet U-Pb ages for hydrothermal skarn garnets, measuring ages for the Shimyoka Fe skarn in Zambia (510–496 Ma) and the Porphyry Mountain Cu skarn in Gaspe, Quebec (~360 Ma). The U concentration for these garnets ranged from 3.0 to 32.3 ppm. The ID-TIMS garnet U-Pb ages are analyzed by completely dissolving the garnet crystal (including any inclusions) and measuring the U and Pb isotopes. If the U content of the garnet is hosted by the inclusions, then the garnet may simply act as a container (DeWolf et al., 1996) in which the low rate of diffusion for U and Pb in garnet protects the inclusions from isotopic resetting due to diffusive Pb loss, reequilibration, recrystallization, or alteration by external fluids (Jung and Mezger, 2003; Lima et al., 2012). In this case, the measured age would be that of the inclusions and not the garnet.

While inclusions are a first-order concern when using the ID-TIMS technique, they are not the sole source of radiogenic elements. Haack and Gramse (1972) investigated the fission track densities of 43 garnets from a suite of skarn samples from around the globe. They found that the U concentrations in andradite and spessartine garnets (estimated as 30–35 ppm) were sufficiently high to potentially determine a fission track age. DeWolf et al. (1996) showed that while grossular-andradite garnets from Cascade Slide (Adirondacks, USA) had little variation in fission track density, indicating that U was homogeneously distributed, the almandine garnets from the Pikwitonei granulite domain (Manitoba, Canada) showed localization of fission tracks around micron-scale monazite inclusions. For these samples the radiogenic elements were largely inclusion hosted. Furthermore, Smith et al. (2004) reported U concentrations of up to 358 ppm in andraditic skarn garnets from the Isle of Skye. These studies suggest that the distribution of U is strongly composition dependent, with the higher abundances possible in grossular-andradite garnet.

The LA-ICP-MS garnet U-Pb dating technique was refined by Seman et al. (2017), who report U-Pb ages for garnets from various tectonics settings with variable grossular-andradite contents, U concentrations, and ages, including Willsboro andradite (~1020 Ma; Adirondacks, USA), Red and Yellow Mali grandite (~200 Ma; Southern Mali), Lake Jaco grossular (~35 Ma; Coahuila, Mexico), and Serifos andradite (~10 Ma; Greece) (see Table 1). Compared to the established techniques, LA-ICP-MS garnet U-Pb dating has the advantage of being an in situ technique; large inclusions can be visually screened out during laser spot selection or during data analysis, only small sample volumes are required, and the closure temperature of the U-Pb system is high relative to other established techniques (e.g., $^{40}Ar/^{39}Ar$; Mezger et al., 1989). Burton et al. (1995) evaluated diffusion of Pb and other cations in garnet and found that Pb does not readily diffuse, even at temperatures up to 900°C, which is higher than U-Pb in monazite (Tc = 725 ± 25°C; Parrish, 1990) and Sm-Nd in garnet (Tc = 600 ± 30°C; Mezger et al., 1992). Hence, garnet U-Pb ages record the timing of garnet growth.

Analytical Techniques

Samples were collected from Big Gossan underground mine drifts and from drill core (Fig. 2). Large garnets (0.3–1 cm in size) were separated from the samples using a chisel, and the fragments were visually inspected for inclusions. Five large crystals were selected from each sample, mounted in epoxy, and polished to expose a clean face of the garnet rim. The sample with the largest garnets, BG14W-07 65m, was selected to date both the core and rim to determine if there was a detectable difference in age. Three garnets from this sample were cut in half using a slow-speed saw and then mounted in epoxy. Backscattered electron (BSE) images were used to evaluate the zoning within the garnet crystals prior to analysis.

Garnet U-Pb analyses were completed at the University of Texas at Austin, Texas, using a single collector ThermoFisher

Table 1. LA-ICP-MS Garnet U/Pb Ages from Seman et al. (2017)

Garnet	Location	Composition (% Grs, % And)	Age (Ma)	Uncertainty (Ma)	U (ppm)
Serifos Andradite	Cyclades, Greece	Grs0, And100	9.15	0.36	9.3
Lake Jaco Grossular	Coahuila, Mexico	Grs84, And16	34	1.4	1.7
Mali Grandite Yellow	Mali, West Africa	Grs72, And28	202	2	2.0
Mali Grandite Red	Mali, West Africa	Grs37, And52	202	2	7.0
Willsboro Andradite	Adirondacks, NY	Grs10, And90	1022	16	1.0

Abbreviations: And = andradite, Grs = grossular, LA-ICP-MS = laser ablation-inductively coupled plasma-mass spectrometry

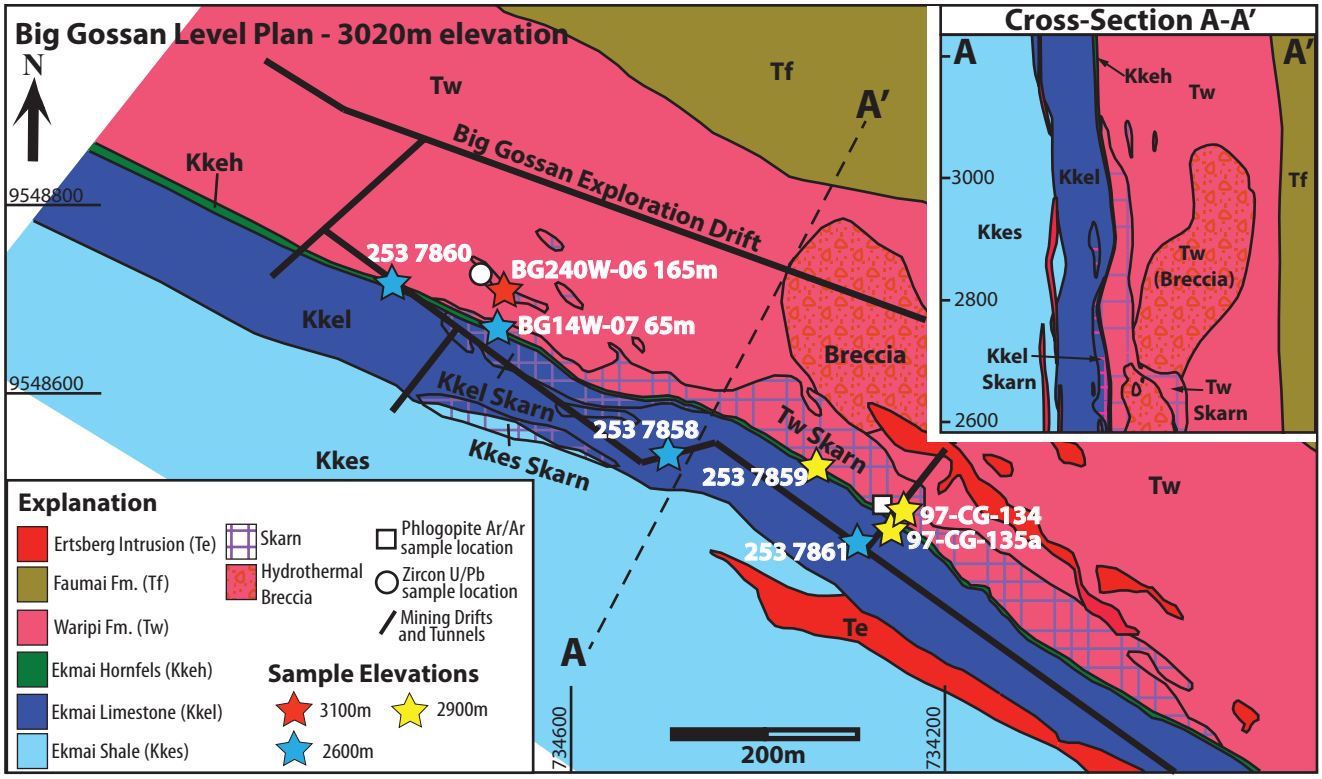

Fig. 2. Level plan of the Big Gossan skarn at 3,020-m elevation. Sample locations are projected onto the level plan with the elevation denoted by color. Approximate location of the phlogopite Ar-Ar sample from Prendergast et al. (2005) is shown. Inset shows a cross section of the Big Gossan skarn orebody from A-A'.

Element2 ICP-MS with an attached PhotonMachine Analyte G.2 19-nm ArF Excimer Laser and large-volume Helex sample cell. The method of Seman et al. (2017) was used to acquire data: garnets were ablated for 30 s (10-Hz repetition rate, 6-mJ energy, 17% beam attenuation, resulting in a fluence rate of 1.67 J/cm^2) using a large 110-µm spot size in order to maximize count rates. The instrument was tuned in order to maximize ^{238}U counts and minimize the interferences from oxide masses (UO <0.5%). In order to determine which primary standard is most appropriate for high U garnets, data reduction was completed twice: once using a Willsboro garnet primary standard (Seman et al., 2017) and once using GJ1, a Sri Lankan zircon primary standard. Although the zircon is not a matrix-matched standard, the wide laser pits (shallow depth) minimize the effects of downhole fractionation, as there were no differences in age when using the first 10 s of the ablation compared to the full 30 s of ablation. Furthermore, the ages calculated using the Willsboro garnet as a primary standard overlapped within error with the ages calculated using GJ1. However, as the propagation of isotopic ratio uncertainties favors GJ1, which has a considerably more precise TIMS calibration, the ages reported here were calculated with GJ1 as the primary standard.

Data were processed using the Iolite software package (Paton et al., 2011) and ages were calculated using Isoplot v. 4 (Ludwig, 1998). Given the heterogeneous distribution of common Pb in the Big Gossan garnets, we use a linear regression in Tera-Wasserburg space, where the lower concordia intercept and its uncertainty are reported as the common Pb-corrected sample age and uncertainty (Tera and Wasserburg, 1972).

Garnet U-Pb Age Results

Eight samples with andradite garnet were selected from various locations across a 600-m lateral and 500-m vertical distance within the skarn (Fig. 2). Meinert et al. (1997) describe the Big Gossan skarn as zoned about a main fluid conduit along the Ekmai-Waripi contact, where proximal zones are garnet rich and pyroxene poor (dark red-brown garnets and pale pyroxenes), intermediate zones contain equal amounts of garnet and pyroxene (brown garnets and green pyroxenes), and distal zones are dominated by dark-green pyroxene and pale-green to brownish garnets. Based on this classification, samples BG-240W-06 165m, BG-14W-07 65m, 97-CG-134, and 97-CG-135a are from proximal skarn zones, whereas samples 2537858, 2537859, 2537860, and 2537861 are from intermediate skarn zones. Descriptions of the skarn protolith, associated skarn gangue minerals, mineralization, and garnet character are reported in Table 2. Compositional zoning from core to rim has been previously noted in Big Gossan garnets (Meinert et al., 1997); therefore, for seven of the eight samples, polished rims were targeted for dating in order to avoid potential complications from analyzing multiple growth zones. BSE images show the garnet surfaces that were targeted (Fig. 3).

Garnet U-Pb age data are reported in the supplementary information. Tera-Wasserburg plots for seven garnet samples show there is one isotopic composition of common Pb, as all

Table 2. Garnet Sample Locations

Sample ID	Sample location	Coordinates			Formation	Protolith	Associated skarn gangue minerals	Associated mineralization	Garnet details
		Easting	Northing	Elevation (m)					
BG240W-06 165m	Drill core	734838	9548716	3,026	Tw	Dolomite	Actinolite-tremolite, diopside, anhydrite, sphalerite, quartz, magnetite	Chalcopyrite, pyrite	Dark reddish-black color, coarse- to very coarse grained
BG14W-07 65m	Drill core	734927	9548464	2,549	Tw	Dolomite	Garnet, chlorite, epidote, magnetite, tremolite, anhydrite	Chalcopyrite, pyrite	Dark reddish-black color, moderate- to coarse-grained
97-CG-134	Drift sample	734837	9548635	3,016	Tw	Dolomite	Garnet, anhydrite, epidote, quartz, calcite, hematite	Chalcopyrite, pyrite	Dark reddish-black color, moderate- to coarse-grained
97-CG-135a	Drift sample	734832	9548645	3,016	Tw	Dolomite	Garnet, tremolite, anhdyrite, epidote, quartz, dolomite, hematite	Chalcopyrite, pyrite	Dark reddish-black color, moderate- to coarse-grained
2537858	BG2640L XC29	734748	9548583	2,647	Tw	Dolomite	Anhydrite, diopside, epidote, sphalerite, magnetite	Chalcopyrite, pyrite	Brown color, coarse- to very coarse grained
2537859	BG2860L XC40	734919	9548523	2,866	Tw	Dolomite	Actinolite-tremolite, garnets, sphalerite, hematite, epidote	Chalcopyrite, pyrite	Brown color, coarse- to very coarse grained
2537860	BG2600L XC15	734562	9548685	2,613	Tw	Dolomite	Diopside, actinolite, tremolite, anhydrite, magnetite	Chalcopyrite, pyrite	Brown color, coarse- to very coarse grained
2537861	BG2560L XC45	734963	9548473	2,568	Tw	Dolomite	Diopside, anhydrite, quartz, epidote, magnetite	Chalcopyrite, pyrite	Greenish-brown color, coarse- to very coarse grained

Abbreviations: Tw = Waripi Formation

Fig. 3. Backscattered electron images of dated garnets. (A) Aggregate of three garnet crystals, each showing two to three growth zones along the rims. White circles show the location of the 110-µm laser pits. (B) Garnet crystal with bright sulfide and dark pyroxene inclusions that were avoided during laser spot selection. White circles show the location of the 110-µm laser pits. (C) Image showing faint zoning within an otherwise compositionally uniform garnet rim. (D) Garnet crystal with dark pyroxene inclusions in the center of the rim. Abbreviations: cpy = chalcopyrite, pyr = pyrite.

of the error ellipses for the 50 to 60 laser spot analyses lie along a single mixing line (Fig. 4). Variations in U and common Pb concentrations result in a spread of data points along the mixing line, allowing for a robust common Pb mixing line to be regressed, such that the reported lower intercept age is precise (errors between 0.03 and 0.2 Ma) (Table 2). The garnet ages overlap within error, and there is no spatial pattern to the ages. Garnet U-Pb ages constrain the time window of Big Gossan skarn formation between 2.72 ± 0.04 and 2.86 ± 0.07 Ma. Even with conservative consideration of the errors, we are confident the Big Gossan skarn was one of the last ore-forming events in the mining district.

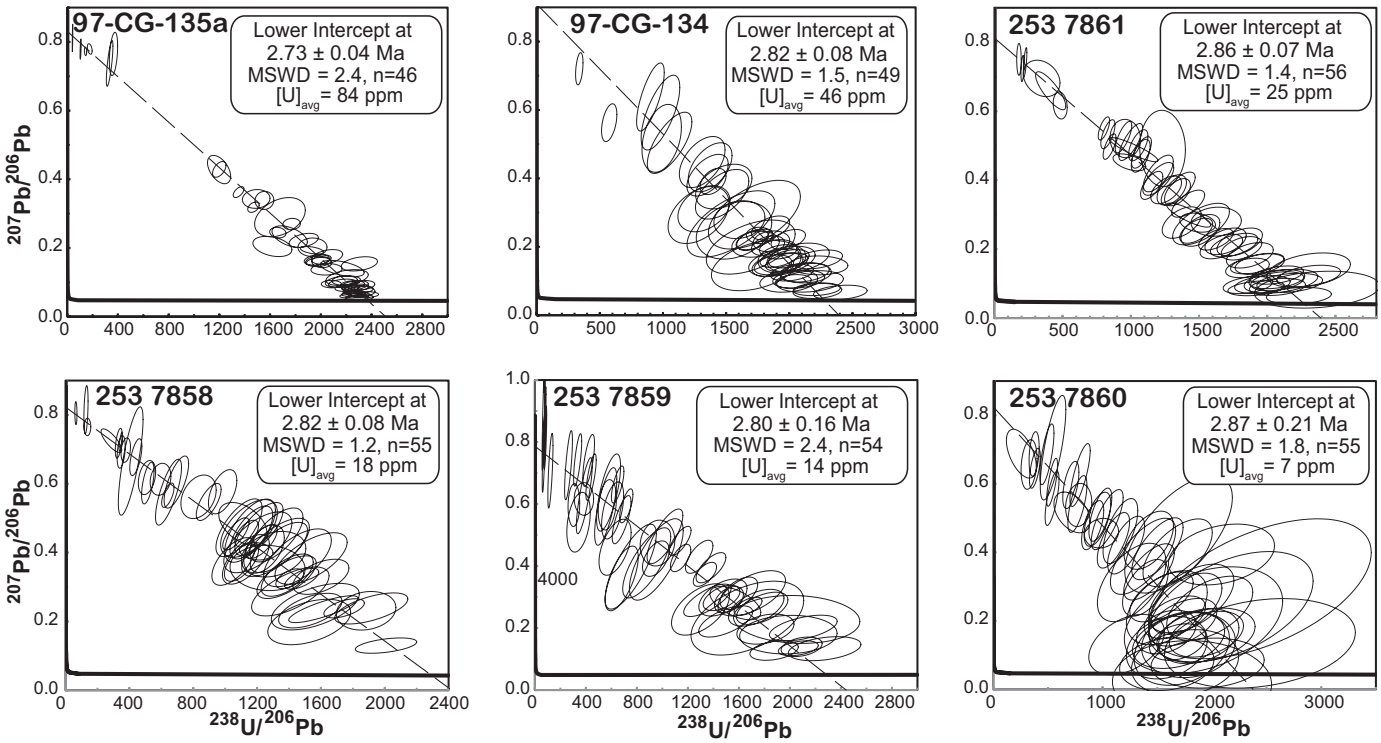

Fig. 4. Tera-Wasserburg diagrams for six of the garnet U-Pb samples. Lower intercept ages are reported. Data-point error ellipses are 2σ. Abbreviations: MSWD = mean square of weighted deviates.

Duplicates

In order to test the reproducibility of the ages two kinds of duplicates were analyzed: (1) one sample was analyzed twice, and (2) two samples from meters apart along the same drift in the Big Gossan skarn were analyzed. Garnets from sample BG-240W-06 165m were dated twice four months apart (January 2016 and April 2016). The ages from each run are 2.75 ± 0.03 Ma (n = 154 spots) and 2.73 ± 0.06 Ma (n = 50 spots) (Fig. 5). The agreement of the age and analytical error is remarkable. Two samples collected ~10 m apart along the same drift, 97-CG-134 and 97-CG-135a, have ages of 2.84 ± 0.11 and 2.72 ± 0.05 Ma, respectively, which overlap within error. Collectively, the ability to reproduce duplicate ages indicates that the garnet U-Pb chronometer is robust and reliable.

Core-rim ages

The andradite garnet U-Pb geochronometer also has the potential to constrain garnet growth rates within a skarn system. Furthermore, dating individual garnet crystals may provide insight into the spatial growth pattern of the skarn system through time. In order to test the ability to measure garnet growth rates, three garnets from sample BG14W-07 65m were cut for central sections. While the core ages trended older for all three garnet crystals analyzed, the core and the rim ages overlap in error (Table 3). Based on compiled core and rim analyses, the cores are 2.78 ± 0.05 Ma and the rims are 2.72 ± 0.04 Ma. While it is not possible to constrain a growth rate for these garnets, the age results suggest that these three garnets formed in at most tens of thousands of years.

External age constraints

The Big Gossan skarn is a good place to test the accuracy of the garnet U-Pb chronometer, as there is excellent age control for the skarn based on field relationships, the phlogopite $^{40}Ar/^{39}Ar$ age, and extensive zircon U-Pb dating throughout the district (Fig. 6). Gregory (2004) mapped fault patterns in the exploration drifts and discovered that while abundant faults are present in the country rock, the skarn exposed in the drifts contains few faults. This indicates the skarn formed late in the faulting history of this part of the district. The phlogopite $^{40}Ar/^{39}Ar$ age of 2.82 ± 0.04 Ma reported by Prendergast et al. (2005) overlaps with the Big Gossan garnet U-Pb ages. Additionally, extensive zircon U-Pb dating in the mining district has constrained the timing of the Grasberg Igneous Complex between 3.6 and 3.1 Ma and the nearby Ertsberg pluton between 3.1 and 2.8 Ma (Wafforn, 2017). Drilling has recovered one strongly altered dike in the Big Gossan area (location shown in Fig. 2). This dike yielded a zircon U-Pb age of 3.0 ± 0.1 Ma, as expected given that the dike predates hydrothermal activity. The 2.9 to 2.7 Ma U-Pb ages for garnets from the Big Gossan skarn are thus in agreement with all external age constraints.

Discussion

One of the advantages of in situ garnet dating is the ability to directly date the timing of skarn garnet crystallization. This is a significant advance compared to the traditional approach of dating the crystallization age of related intrusions (if one can easily be identified) and the $^{40}Ar/^{39}Ar$ cooling age of skarn minerals such as phlogopite, biotite, or K-feldspar. All

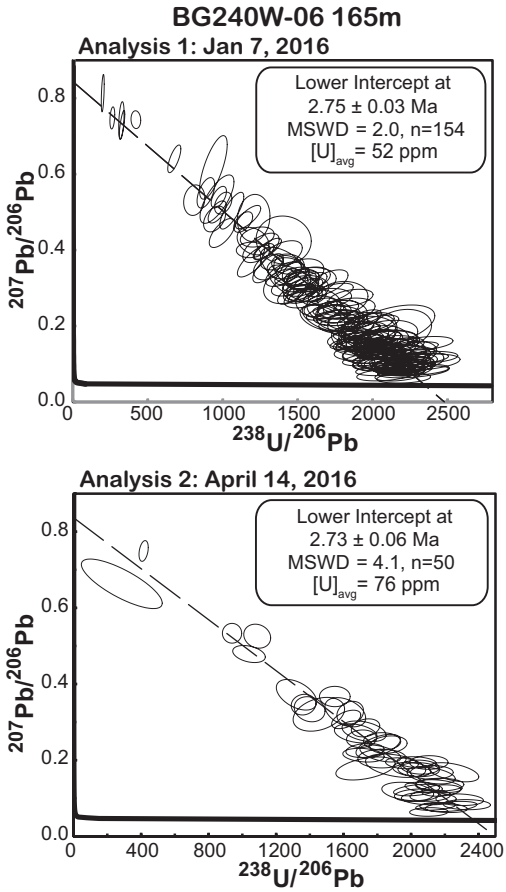

Fig. 5. Tera-Wasserburg diagrams for the duplicate analyses of sample BG240W-06 165m. Both of the ages overlap within error. Data-point error ellipses are 2σ. Abbreviations: MSWD = mean square of weighted deviates.

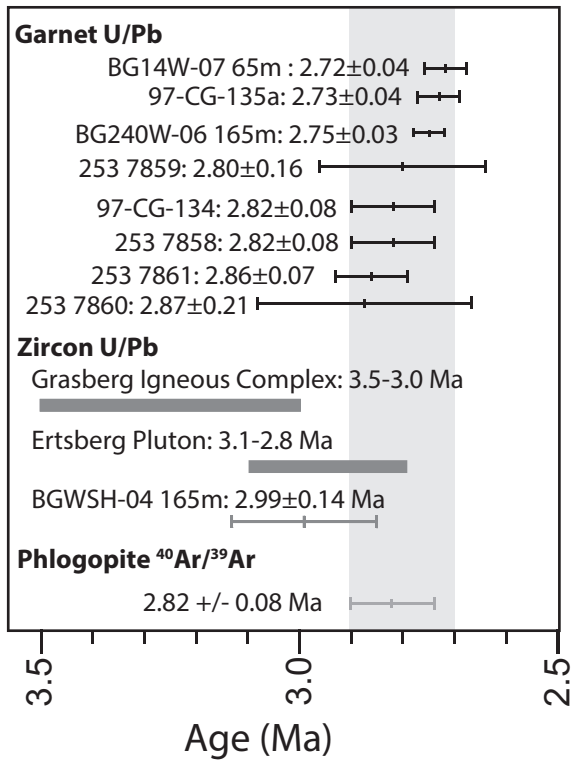

Fig. 6. Summary plot showing the external age constraints for the garnet U-Pb ages. Zircon U-Pb ages from Wafforn (2017), sample BG WSH-04 165m from a hydrothermally altered dike that predates the Big Gossan skarn, and phlogopite $^{40}Ar/^{39}Ar$ ages from Prendergast et al. (2005). Shaded gray bar from 2.9 to 2.7 Ma shows the age range of the Big Gossan skarn based on the garnet U-Pb ages. All ages shown with 2σ error.

of the garnet crystallization ages reported here fall within a time period between 2.72 ± 0.04 and 2.86 ± 0.07 Ma, with an apparent duration of hydrothermal fluid flow of 30 to 250 k.y. (Fig. 6). The age results for Big Gossan do not show a systematic spatial pattern. However, as the precision is reported to as good as ±0.03 m.y., the possibility remains that a finer-scale sampling may put new constraints on the spatial evolution of this skarn body.

Table 3. Age Results for Core and Rim Analyses of Three Garnets from Sample BG14W-07 65m

		Age (Ma)	Uncertainty (Ma)	MSWD	No. of spots
Grain 1	Core	2.74	0.10	2.4	25
	Rim	2.73	0.04	1.4	25
Grain 2	Core	2.75	0.09	1.3	25
	Rim	2.70	0.09	2.2	25
Grain 3	Core	2.83	0.10	1.9	25
	Rim	2.73	0.06	1.5	25
Compiled	Core	2.78	0.05	2.0	75
	Rim	2.72	0.04	1.7	75

MSWD = mean square of weighted deviates

U and Pb in garnet

One of the additional benefits of in situ garnet U-Pb dating is the ability to map the U distribution. The U concentration in the dated Big Gossan garnets ranges from 10 to 100 ppm, whereas Th concentrations are significantly lower, typically <1 ppm. The observation that U can be homogeneously distributed in the garnet rims makes them a feasible target for LA-ICP-MS U-Pb dating (Fig. 7).

There are two possibilities that could explain the homogeneous distribution of U in the Big Gossan garnets: it could occur in microinclusions that are uniformly distributed throughout the garnets or it could be hosted stoichiometrically in the garnet. While microinclusions cannot be ruled out, none were visible or detected in environmental scanning electron microscope (ESEM) images. The homogeneous distribution of U, as mapped in the laser spots (Fig. 7), suggests that the U is stoichiometric. Meinert et al. (1997) report that garnets from the Big Gossan skarn can be near-end-member andradite ($Ca_3Fe_2[SiO_4]_3$), and DeWolf et al. (1996) found that andradite-rich garnets are more likely to have higher concentrations of REE, U, and Th, suggesting that the larger atomic size of Fe^{3+} relative to Al^{3+} may permit substitution of the larger cations. Naturally occurring U-bearing garnets, named elbrusite-(Zr), have a chemical formula of $Ca_3U_xZr_{(2-x)}Fe_3O_{12}$. Guo et al. (2016) synthesized U-bearing garnets and using X-ray photoelectron and

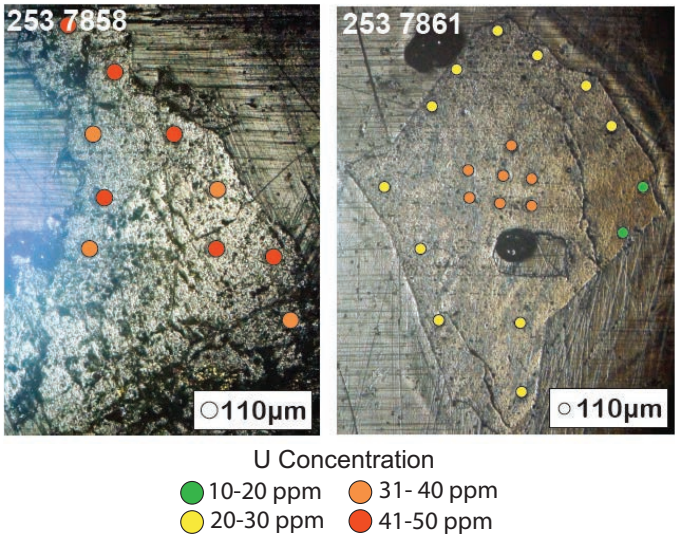

Fig. 7. Reflected light images from samples 253 7858 and 253 7861 showing the location of laser spots on the polished garnet rims. Each spot is color coded based on the measured U concentration.

absorption spectroscopies determined that U occurred in a pentavalent and hexavalent oxidation state. Using transmission ^{57}Fe Mossbauer spectroscopy, they also show that the iron is tetrahedrally coordinated as Fe^{3+}. Based on these results it seems plausible that U occurs in the octahedral site within the Big Gossan andradite garnets.

Lead in the garnets is clearly a mix of common Pb and radiogenic Pb (see Tera-Wasserburg diagrams, Fig. 4). In this case, the consistent isotopic composition of the common Pb and the variation in the concentration of Pb in the garnet crystal creates a spread in the data that forms a single mixing line in Tera-Wasserburg space. The y-intercept on the Tera-Wasserburg diagram represents the ^{207}Pb/^{206}Pb ratio for common Pb in the system: the ~0.86 value is consistent with feldspar and whole-rock common Pb ratios for the district (M. Cloos, unpub. data, 2016).

Future applications

The major requirements for obtaining a garnet U-Pb age are grossular-andradite composition, sufficient concentrations of U to produce measurable radiogenic Pb, and either a lack of common Pb or a consistent isotopic composition of common Pb. Based on the results of this study and previous work by Mezger et al. (1989), Meinert et al. (2001), and Seman et al. (2017), it is possible to measure the ages of skarn garnets from a wide variety of tectonic settings and time periods. Currently, the oldest garnet U-Pb age measured using the LA-ICP-MS technique is 1 Ga, but there is no reason that even older garnets cannot be dated. Based on the current data set, garnets less than 10 Ma require ~5 ppm U to determine a precise garnet U-Pb age, whereas for garnets older than 10 Ma the required U concentration decreases to ~1 ppm U. As the age uncertainty is inversely correlated with the U concentration, the higher the U concentration the better the likelihood of determining a garnet U-Pb age. Further studies are required to determine the full range of possibilities for dating skarn garnets; however, this study shows that with sufficient U and a consistent common Pb composition, it is possible to date garnets with remarkable precision.

Conclusions

All of the andradite garnet U-Pb ages for the Big Gossan skarn are between 2.9 and 2.7 Ma, confirming that the Big Gossan skarn is one of the last major ore-forming events in the Ertsberg-Grasberg mining district. The remarkable agreement between Big Gossan andradite garnet U-Pb ages and external age constraints and the ability to replicate ages provide good evidence that the andradite garnet U-Pb chronometer can be a robust dating technique. Furthermore, the ability to directly date the timing of prograde hydrothermal skarn formation is a significant addition to the geochronologist's toolkit in skarn systems. Based on the results presented here, the prerequisites for precise and robust andradite garnet U-Pb ages for garnets that are ~3 Ma are >5 ppm U and a single, consistent isotopic composition for the common Pb.

Acknowledgments

The authors thank Sugeng Widodo, George MacDonald, Paul Warren, and Wahyu Sunyoto of Freeport, as well as Lisa Stockli for their assistance and input throughout this project. Reza Al Furqan, Pandji Muhammad, Apun Permana, Nimrod Msen, and Heri Purwanto are also thanked for their help in the Freeport core shed. Jacob Makis provided great assistance during sample preparation and analysis. Massimo Chiaradia and Larry Meinert are thanked for their thorough and insightful reviews. Finally, this work would not have been possible without the continued logistical and financial support of Freeport McMoRan, Ertsberg Project Contribution No. 32.

REFERENCES

Arribas, A., Hedenquist, J.W., Itaya, T., Okada, T., Concepcion, R.A., and Garcia, J.S., 1995, Contemporaneous formation of adjacent porphyry and epithermal Cu-Au deposits over 300 ka in northern Luzon, Philippines: Geology, v. 23, p. 337–340.

Ballard, J.R., Palin, J.M., Williams, I.S., Campbell, I.H., and Faunes, A., 2001, Two ages of porphyry intrusion resolved for the super-giant Chuquicamata copper deposit of northern Chile by ELA-ICP-MS and SHRIMP: Geology, v. 29, p. 383–386.

Baxter, E.F., and Scherer, E.E., 2013, Garnet geochronology: Timekeeper of tectono-metamorphic processes: Elements, v. 9, p. 433–438.

Burnham, C.W., 1979, Magmas and hydrothermal fluids, *in* Barnes, H.L., ed., Geochemistry of hydrothermal ore deposits, New York, Wiley, p. 71–136.

Burton, K.W., and O'Nions, R.K., 1991, High-resolution garnet chronometry and the rates of metamorphic processes: Earth and Planetary Science Letters, v. 107, p. 649–671.

Burton, K.W., Kohn, M.J., Cohen, A.S., and O'Nions, R.K., 1995, The relative diffusion of Pb, Nd, Sr, and O in garnet: Earth and Planetary Science Letters, v. 133, p. 199–211.

Candela, P.A., 1989, Magmatic ore-forming fluids: Thermodynamic and mass transfer calculations of metal concentrations: Reviews in Economic Geology, v. 4, p. 203–221.

Candela, P.A., and Holland, H.D., 1984, The partitioning of copper and molybdenum between silicate melts and aqueous fluids: Geochimica et Cosmochimica Acta, v. 48, p. 373–380.

Chiaradia, M., Vallance, J., Fontboté, L., Stein, H., Schaltegger, U., Coder, J., Richards, J., Villeneuve, M., and Gendall, I., 2009, U-Pb, Re-Os, and ^{40}Ar/^{39}Ar geochronology of the Nambija Au skarn and Pangui porphyry Cu deposits, Ecuador: Implications for the Jurassic metallogenic belt of the Northern Andes: Mineralium Deposita, v. 44, p. 371–387.

Cline, J.S., and Bodnar, R.J., 1991, Can economic porphyry copper mineralization be generated by a typical calc-alkaline melt?: Journal of Geophysical Research, v. 96, p. 8113–8126.

Cloos, M., 2001, Bubbling magma chambers, cupolas, and porphyry copper deposits: International Geology Reviews, v. 43, p. 285–311.
Cloos, M., and Sapiie, B., 2013, Porphyry copper deposits: Strike-slip faulting and throttling cupolas: International Geology Reviews: v. 55, p. 43–65.
Deckart, K., Clark, A.H., Celso, A.A., Ricardo, V.R., Bertens, A.N., Mortensen, J.K., and Fanning, M., 2005, Magmatic and hydrothermal chronology of the giant Rio Blanco porphyry copper deposit, Central Chile: Implications of an integrated U-Pb and $^{40}Ar/^{39}Ar$ database: Economic Geology, v. 100, p. 905–934.
Deng, X.D., Li, J., and Wen, G., 2015, U-Pb geochronology of hydrothermal zircons from the Early Cretaceous iron skarn deposits in the Handan-Xingtai district, North China craton: Economic Geology, v. 110, p. 2159–2180.
DeWolf, C.P., Zeissler, C.J., Halliday, A.N., Mezger, K., and Essene, E.J., 1996, The role of inclusions in U-Pb and Sm-Nd garnet geochronology: Stepwise dissolution experiments and trace uranium mapping by fission track analysis: Geochimica et Cosmochimica Acta, v. 60, p. 121–134.
Gregory, C.H., 2004, Subsurface meso-scale structural geology and petrology near Big Gossan orebody, Ertsberg (Gunung Bijih) mining district, Irian Jaya, Indonesia: M.S. thesis, Austin, Texas, University of Texas at Austin, 253 p.
Guo, X., Navrotsky, A., Kukkadapu, R.K., Engelhard, M.H., Lanzirotti, A., Newville, M., Ilton, E.S., Sutton, S.R., and Xu, H., 2016, Structure and thermodynamics of uranium-containing iron garnets: Geochimica et Cosmochimica Acta, v. 189, p. 269–281.
Haack, U.K., and Gramse, M., 1972, Survey of garnets for fossil fission tracks: Contributions to Mineralogy and Petrology, v. 34, p. 258–260.
Hedenquist, J.W., and Lowenstern, J.B., 1994, The role of magmas in the formation of hydrothermal ore deposits: Nature, v. 370, p. 519–527.
Jung, S., and Mezger, K., 2003, U-Pb garnet chronometry in high-grade rocks—case studies from the central Damara orogeny (Namibia) and implications for the interpretation of Sm-Nd garnet ages and the role of high U-Th inclusions: Contributions in Mineralogy and Petrology, v. 146, p. 382–396.
Leys, C.A., Cloos, M., New, B.T.E., and MacDonald, G.D., 2012, Copper-gold ± molybdenum deposits of the Ertsberg-Grasberg district, Papua, Indonesia: Society of Economic Geologists, Special Publication 16, p. 215–235.
Lima, S.M., Corfu, F., Neiva, A.M.R., and Ramos, J.M.F., 2012, U-Pb ID-TIMS dating applied to U-rich inclusions in garnet: American Mineralogist, v. 97, p. 800–806.
Ludwig, K.R., 1998, On the treatment of concordant uranium-lead ages: Geochimica et Cosmochimica Acta, v. 62, p. 665–676.
Maksaev, V., Munizaga, F., McWilliams, M., Fanning, M., Mathur, R., Ruiz, J., and Zentilli, M., 2004, New chronology for El Teniente, Chilean Andes, from U-Pb, $^{40}Ar/^{39}Ar$, Re-Os, and fission-track dating: Implications for the evolution of a supergiant porphyry Cu-Mo deposit: Society of Economic Geologists, Special Publication 11, p. 15–54.
Marsh, T.M., Einaudi, M.T., and McWilliams, M., 1997, $^{40}Ar/^{39}Ar$ Geochronology of Cu-Au and Au-Ag mineralization in the Potrerillos District, Chile: Economic Geology, v. 92, p. 784–806.
McDowell, F.W., McMahon, T.P., Warren, P.Q., and Cloos, M., 1996, Pliocene Cu-Au bearing igneous intrusions of the Gunung Bijih (Ertsberg) district, Irian Jaya, Indonesia: K-Ar Geochronology: Journal of Geology, v. 104, p. 327–340.
Meinert, L.D., Hefton, K.K., Mayes, D., and Tasiran, I., 1997, Geology, zonation, and fluid evolution of the Big Gossan Cu-Au skarn deposit, Ertsberg district, Irian Jaya: Economic Geology, v. 92, p. 509–534.
Meinert, L.D., Nicolescu, S., Mortensen, J.K., and Cornell, D.H., 2001, U-Pb dating of hydrothermal garnet from skarn deposits—implications for petrogenesis and ore deposits: Geological Society of America, Abstracts with Programs, v. 33, p. A130.
Meinert, L.D., Hedenquist, J.W., Satoh, H., and Matsuhisa, Y., 2003, Formation of anhydrous and hydrous skarn in Cu-Au ore deposits by magmatic fluids: Economic Geology, v. 98, p. 147–156.
Meinert, L.D., Dipple, G., and Nicolescu, S., 2005, World skarn deposits: Economic Geology 100th Anniversary Volume, p. 299–336.
Mertig, H.J., Rubin, J.N., and Kyle, J.R., 1994, Skarn Cu-Au orebodies of the Gunung Bijih (Ertsberg) district, Irian Jaya, Indonesia: Journal of Geochemical Exploration, v. 50, p. 179–202.
Mezger, K., Hanson, G.N., and Bohlen, S.R., 1989, U-Pb systematics of garnet: Dating the growth of garnet in the Late Archean Pikwitonei granulite domain at Cauchon and Natawahunan Lakes, Manitoba, Canada: Contributions to Mineralogy and Petrology, v. 101, p. 136–148.
Mezger, K., Essene, E.J., and Halliday, A.N., 1992, Closure temperatures of the Sm-Nd system in metamorphic garnets: Earth and Planetary Science Letters, v. 113, p. 397–409.
Parrish, R.R., 1990, U-Pb dating of monazite and its application to geological problems: Canadian Journal of Earth Sciences, v. 27, p. 1435–1450.
Paterson, J.T., and Cloos, M., 2005, Grasberg porphyry Cu-Au deposit, Papua, Indonesia: 1. Magmatic history *in* Porter, T.M., ed., Super porphyry copper and gold deposits: A global perpspective: Adelaide, PCG Publishing, p. 313–329.
Paton, C., Hellstrom, J., Paul, B., Woodhead, J., and Hergt, J., 2011, Iolite: Freeware for the visualization and processing of mass spectrometric data: Journal of Analytical Atomic Spectrometry, v. 26, p. 2508–2518.
Peng, J., Zhou, M.F., Hu, R., Shen, N., Yuan, S., Bi, X., Du, A., and Qu, W., 2006, Precise molybdenite Re-Os and mica Ar-Ar dating of the Mesozoic Yaogangxian tungsten deposit, central Nanling district, South China: Mineralium Deposita, v. 41, p. 661–669.
Prendergast, K., Clarke, G.W., Pearson, N.J., and Harris, K., 2005, Genesis of pyrite-Au-As-Zn-Bi-Te zones associated with Cu-Au skarns: Evidence from Big Gossan and Wanagon gold deposits, Ertsberg district, Papua, Indonesia: Economic Geology, v. 100, p. 1021–1050.
Scherer, E.E., Cameron, K.L., and Blichert-Toft, J., 2000, Lu-Hf garnet geochronology: Closure temperature relative to the Sm-Nd system and the effects of trace mineral inclusions: Geochimica et Cosmochimica Acta, v. 64, p. 3413–3432.
Seman S., Stockli, D.F., and McLean N.M., 2017, U-Pb geochronology of grossular-andradite garnet: Chemical Geology, v. 460, p. 106–116.
Shinohara, H., Iiyama, J.T., and Matsuo, S., 1989, Partition of chlorine compounds between silicate melt and hydrothermal solutions: 1. Partition of NaCl-KCl: Geochimica et Cosmochimica Acta, v. 53, p. 2617–2630.
Sillitoe, R.H., 1993, Epithermal models: Genetic types, geometric controls, and shallow features: Geological Association of Canada Special Paper 40, p. 403–417.
——2010, Porphyry copper systems: Economic Geology, v. 105, p. 3–41.
Smit, M.A., Scherer E.E., and Mezger, K., 2013, Lu-Hf and Sm-Nd garnet geochronology: Chronometric closure and implications for dating petrological process: Earth and Planetary Science Letters, v. 381, p. 222–233.
Smith, M.P., Henderson, P., Jeffries, T.E.R., Long, J., and Williams, C.T., 2004, The rare earth elements and uranium in garnets from the Beinn an Dubhaich aureole, Skye, Scotland, UK: Constraints on processes in a dynamic hydrothermal system: Journal of Petrology, v. 45, p. 467–484.
Tera, F., and Wasserburg, G.J., 1972, U-Th-Pb systematics in three Apollo 14 basalt and the problem of initial Pb in lunar rocks: Earth and Planetary Science Letters, v. 14, p. 281–304.
Titley, S.R., 1975, Geological characteristics and environment of some porphyry copper occurrences in the southwestern Pacific: Economic Geology, v. 70, p. 499–514.
von Quadt, A., Erni, M., Matinek, K., Moll, M., Peytcheva, I., and Heinrich, C.A., 2011, Zircon crystallization and the lifetimes of ore-forming magmatic-hydrothermal systems: Geology, v. 39, p. 731–734.
Wafforn, S., 2017, Geo- and thermochronology of the Ertsberg-Grasberg Cu-Au mining district, west New Guinea, Indonesia: Ph.D. dissertation, Austin, Texas, University of Texas at Austin, 357 p.
Wan, B., Xiao, W., Han, C., Windley, B.F., Zhang, L., Qu, W., and Du, A., 2014, Re-Os molybdenite age of the Cu-Mo skarn ore deposit at Suoerkuduke in East Junggar, NW China, and its geological significance: Ore Geology Reviews, v. 56, p. 541–548.
Wang, J.Z., Li, J.W., Zhao, X.F., Ma, C.Q., Qu, W.J., and Du, A.D., 2008, Re-Os dating of pyrrhotite from the Chaoshan gold skarn, eastern Yangtze craton, eastern China: International Geology Reviews, v. 50, p. 392–406.
Xie, G., Mao, J., Zhao, H., and Yao, L., 2012, Zircon U-Pb and phlogopite $^{40}Ar/^{39}Ar$ age of the Chengchao and Jinshandian skarn Fe deposits, southeast Hubei province, middle-lower Yangtze River Valley metallogenic belt, China: Mineralium Deposita, v. 47, p. 633–652.
Zhao, W.W., Zhou, M.F., and Chen, W.T., 2016, Growth of hydrothermal baddeleyite and zircon in different stages of skarnization: American Mineralogist, v. 101, p. 2689–2700.
Zhu, J.J., Hu, R., Richards, J.P., Bi, X., and Zhong, H., 2015, Genesis and magmatic-hydrothermal evolution of the Yangla skarn Cu deposit, southwest China: Economic Geology, v. 110, p. 631–652.

Stephanie Wafforn is currently a senior project geologist with Pretium Resources, focused on gold exploration in British Columbia's Golden Triangle. She received a Ph.D. degree from The University of Texas at Austin (USA) in 2017, a master's degree from Oregon State University (USA) in 2013, and a bachelor's degree from Queen's University (Canada) in 2011. Stephanie's research interests include understanding the temporal and spatial evolution of magmatic-hydrothermal ore systems and developing new models and tools for successful mineral exploration.